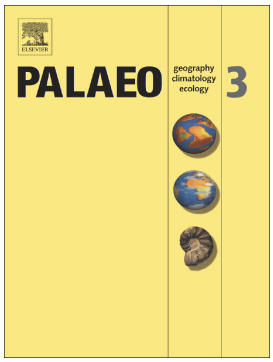

Tracking drainage basin evolution, continental tectonics, and climate change: Implications from osmium isotopes of lacustrine systems

Jeffrey T. Pietras, David Selby, Ryan Brembs, Abby Dennett

PII: S0031-0182(19)30721-7

DOI: https://doi.org/10.1016/j.palaeo.2019.109471

Reference: PALAEO 109471

To appear in: *Palaeogeography, Palaeoclimatology, Palaeoecology*

Received date: 31 July 2019

Revised date: 14 November 2019

Accepted date: 14 November 2019

Please cite this article as: J.T. Pietras, D. Selby, R. Brembs, et al., Tracking drainage basin evolution, continental tectonics, and climate change: Implications from osmium isotopes of lacustrine systems, *Palaeogeography, Palaeoclimatology, Palaeoecology* (2018), https://doi.org/10.1016/j.palaeo.2019.109471

Tracking drainage basin evolution, continental tectonics, and climate change: Implications from osmium isotopes of lacustrine systems

Jeffrey T Pietras[1], David Selby[2,3], Ryan Brembs[1], Abby Dennett[1]

[1]Department of Geological Sciences, Binghamton University, 4400 Vestal Pkwy E, Binghamton, NY 13902, USA

[2]Department of Earth Sciences, Durham University, Stockton Road, Durham DH1 3LE, UK

[3]State Key Laboratory of Geological Processes and Mineral Resources, School of Earth Resources, China University of Geosciences, Wuhan, 430074 Hubei, China

ABSTRACT

Organic matter in the lacustrine Eocene Green River Formation in two cores separated by 16 km in the Uinta Basin record similar centimeter-scale initial $^{187}Os/^{188}Os$ (denoted as Os_i) stratigraphic profiles. This demonstrates that the Os isotopic composition of lacustrine organic matter is spatially homogeneous and in this case documents variation on the time scale of thousands of years. The Os_i stratigraphy developed here indicates temporal change in the Os isotopic composition of lake water which is regulated by the Os isotopic composition of inflowing chemical weathering products from the surrounding drainage basin. Although observed Os_i variability is just above the level of analytical uncertainty, it can be modeled with less than a 6% change in water input from radiogenic to nonradiogenic sources. This highlights the sensitivity of this isotopic tracer. Changes in Os isotope composition may reflect changes in relative discharge of rivers with different Os isotope composition, changes in the footprint of the drainage area to include or exclude different rock types, or unroofing. Thus, this study suggests that Os isotope

stratigraphy in lacustrine settings can be used to link basin stratigraphy to changes in the drainage basin which are driven by climatic, tectonic, and geomorphic processes.

The similarity in Os isotope stratigraphy between the two cores documented here highlights its utility for detailed chronostratigraphic correlation within and between lacustrine basins. A conservative sedimentation rate suggests that Os_i in these lacustrine deposits changed at a rate of ~0.01 per kiloyear, two orders of magnitude faster than has been reported in marine organic-rich sedimentary rocks (Ravizza, 2007). Furthermore, linear regression of $^{187}Re/^{188}Os$ and $^{187}Os/^{188}Os$ ratios of all samples yields a Model 3 depositional age determination of 48.3 ± 2.8 Ma (2σ, MSWD = 8.2) which statistically indistinguishable from a weighted mean laser fusion $^{40}Ar/^{39}Ar$ sanidine age of 49.58 ± 0.32 Ma (Smith and Carroll, 2015) of a temporally adjacent volcanic ash.

1. Introduction

Lacustrine deposits record paleoclimate, paleoecology, vertebrate and invertebrate evolution, tectonic activity, and landscape change; and are also important sources of energy and mineral resources (Katz, 1990; Gierlowski and Kelts, 2000). Due to their small volume compared to the surrounding drainage basin, lakes tend to respond noticeably to even minor changes in sediment supply, water balance, and inflow water chemistry. This unique behavior can provide high-resolution records of geologic processes such as climate change, tectonic activity, and geomorphic landscape evolution within the continental setting, disconnected from the globally averaged record of marine strata. Unfortunately, many lacustrine deposits lack robust chronostratigraphic markers needed to link basin stratigraphy with climatic, tectonic, or geomorphic driving mechanisms. For example, Barremian and Aptian syn-rift lacustrine mudstones present along the Brazilian Atlantic margin (Rangel and Carminatti, 2000; Berman, 2008) also exist on the less-studied conjugate margin of Angola and Namibia. Although tectonic restorations

(e.g. de Wit et al., 2008; Moulin et al., 2010; Quirk et al., 2013) and depositional environment reconstructions (Chaboureau et al., 2013) depict possible hydrologic connections, concrete chronostratigraphic correlations are lacking. Additionally, the preponderance of mudstones in lacustrine basins hinders sediment provenance approaches, such as sandstone petrography or detrital zircon geochronology, that require a coarse-grained fraction. However, chemical and organic precipitates, common in lacustrine deposits, provide an ideal scenario for the use of time varying geochemical tracers. Proxies such as Sr and Os isotopes, delivered to the lake in the dissolved load, can be chronostratigraphic and provenance indicators in these settings. The $^{87}Sr/^{86}Sr$ composition in lacustrine carbonates have been used to investigate water provenance, drainage basin unroofing, hydrologic connections between basins, and as chronostratigraphic markers within basins (e.g. Rhodes et al., 2002; Gierlowski-Kordesch et al., 2008; Doebbert et al., 2014; Baddouh et al., 2017). The Re-Os isotopic system of sedimentary organic matter has the potential to provide a higher resolution chemostratigraphic and provenance indicator, and additionally can yield direct radiogenic age control (Ravizza and Turekian, 1989; Cohen et al., 1999; Selby and Creaser, 2003; Selby and Creaser, 2005; Peucker-Ehrenbrink and Ravizza, 2012; Rooney et al., 2012; Du Vivier et al., 2015; and references therein). However, only a few studies have examined the Re-Os isotope system in lacustrine and terrestrial settings (e.g. Peucker-Ehrenbrink and Jahn, 2001; Creaser et al., 2008; Poirier and Hillaire-Marcel, 2011; Cumming et al., 2012; Zaiss et al., 2014, Xu et al., 2017).

Marine $^{187}Os/^{188}Os$ stratigraphy records short-lived events such as glacial-interglacial cycles, meteorite impacts, volcanic eruptions, basin restrictions, and intervals of oceanic anoxia due to the short marine residence time of Os (1-60 kyrs; Peucker-Ehrenbrink and Ravizza, 2000; Peucker-Ehrenbrink and Ravizza, 2012; Du Vivier et al., 2014; Rooney et al., 2016; and references therein). This differentiates Os from Sr, which exhibits a much longer seawater residence time (~10^6 years; Jones and Jenkyns, 2001; McArthur et al., 2012). In a lacustrine setting the residence

time for Sr has been shown to be only 10^3-10^4 years (Doebbert et al., 2014). If the residence time of Os is similarly reduced, then Os_i stratigraphy may record variations at timescales of 10^2-10^3 years or less.

This study investigates the stratigraphic variability of Os_i in a single oil shale bed in the Lower Parachute Creek Member of the Eocene Green River Formation using two cores separated by 16 km in the eastern Uinta Basin. We demonstrate that Os_i is consistent between the two cores, indicating well mixed waters and change in the Os isotopic composition of the paleolake water through time. The estimated rapid (0.01 per kyr) change in Os_i values, and minimal change in water provenance required to yield this change, suggests that the residence time was short, and that Os isotope stratigraphy can provide a very sensitive tracer of drainage basin evolution and hydrological connections between chains of lakes.

2. Geologic setting

The Uinta Basin (Fig. 1) is one in a series of Laramide basins, including the Greater Green River Basin in Wyoming and the Piceance Creek Basin in Colorado, that were filled by large long-lived lakes during the Early to Middle Eocene recorded by deposition of the Green River Formation (Hayden, 1869; Johnson, 1992; Smith et al., 2008). The Green River Formation of the Uinta Basin was deposited in Lake Uinta. The basin is bounded to the north by the Uinta Mountains which expose Precambrian quartzite and shale in the core of the uplift and Paleozoic and Mesozoic carbonate and siliciclastic units on the flanks. Mesozoic siliciclastics are the primary bedrock exposed to the south and southeast in the San Rafael and Uncompahgre uplifts, respectively. However, some older sedimentary units and Precambrian meta-plutonic rocks are also exposed there. The western limit of the basin is defined by the Sevier fold and thrust belt composed of Phanerozoic sedimentary formations with some Cenozoic intrusive and extrusive igneous rocks.

Paleogeographic reconstructions indicate that the general configuration of highlands around the basin were similar to their present configuration during the Eocene (Dickinson et al., 1988; Smith et al., 2008). Thus, the modern drainage basin provides an analogue for Eocene weathering products into Lake Uinta.

The Lower Parachute Creek Member is marked by a repetitive stacking of lithofacies interpreted to represent lake expansion-contraction cycles 15 to 200 cm thick (Brembs, 2017). The base of a typical cycle (Fig. 2) contains a thin bed of brecciated carbonate mudstone intraclasts, oolitic and ostracodal grainstones, or stromatolites, commonly on top of a desiccation surface, erosional scour, or carbonate hard ground. This deposit is interpreted as a transgressive lag formed in the shallow wave-dominated environment during lake level rise. Micro-laminated organic-rich mudstone, termed oil shale deposited in the deeper water environment below wave base, typically overlies the basal bed. Organic matter can be preserved in these beds due to oxygen depletion in stagnant bottom waters (Demaison, and Moore, 1980). Oil shale beds grade upwards into planar and wavy-laminated calcareous, non-organic, mudstone beds that contain an upward increase in burrows, desiccation cracks, and grain size. These features indicate shallowing water depth associated with lake contraction. Since cycle boundaries represent discrete flooding events, they provide time lines that can be used for chronostratigraphic correlation.

Cycles in the Lower Parachute Creek Member of the Uinta Basin are similar to those described in the contemporaneous Green River Formation of Wyoming (e.g. Rhodes et. al, 2002; Pietras and Carroll, 2006), and may have been deposited over similar timescales. Studies using the average spectral misfit approach (Meyers, 2008), simple calculations of stratigraphic thickness or the number of cycles between volcanic tuffs of know age (Pietras et al., 2003; Smith et al., 2003), and spectral analysis constrained by volcanic tuffs age models (Aswasereelert et al., 2013; Machlus et al., 2015) indicate that cycles in the Wilkins Peak Member of the Green River Formation in Wyoming were likely deposited over time periods of 20,000 years or less.

3. Materials and methods

3.1 Samples

Samples were collected from a correlatable oil shale bed in the R4 zone of the Lower Parachute Creek Member in the Skyline 16 (39° 52' 14.4336" N, 109° 06' 44.1678" W) and PR15-7c (39° 59' 26.6424" N, 109° 00' 59.4760" W) cores (Fig. 1) stored at the Utah Core Research Center in Salt Lake City, Utah. Chronostratigraphic correlations between these two cores are robust in the Lower Parachute Creek Member, and are based on the meter-scale cycles described above, decameter-scale organic-rich (R) and organic-lean (L) zones, and volcanic tuffs (Johnson, 1989; Birgenheier and Vanden Berg, 2011; Brembs, 2017). The sampled bed is positioned two lake expansion-contraction cycles above the Skyline ash in both cores, which has a weighted mean laser fusion $^{40}Ar/^{39}Ar$ sanidine age of 49.58 ± 0.32 Ma (Smith and Carroll, 2015). The R4 oil shale studied here contains a second volcanic tuff in both cores, the upper Skyline ash, providing further evidence of temporal equivalence.

Five-centimeter-thick samples were collected at 5 cm spacing such that a near continuous stratigraphic interval was sampled. Twelve samples were collected from the Skyline 16 core and 7 from the PR15-7c core (Table 1). Based on a depositional period of 20,000 years for a complete cycle, instantaneous deposition of the upper Skyline ash, and the estimate that oil shale accumulates at about a third the rate of other facies in the Green River Formation (Smith et al., 2003), the sampled interval represents about 15,000 years, and each sample represents roughly 1,500 years (Fig. 3). This calculation yields a sedimentation rate of 3.4 cm/kyr for oil shale, and 10.2 cm/kyr for the other facies. These results are comparable to average sedimentation rates calculated for members of the Green River Formation in Wyoming based on the average spectral

misfit approach (16.95 cm/kyr; Meyers, 2008) and stratigraphic thicknesses between volcanic tuffs with known ages (8.5 cm/kyr for the Tipton Member, 22.5 cm/kyr for the Wilkins Peak Member, and 11 cm/kyr for the Laney Member; Pietras and Carrol, 2003).

3.2 Re and Os isotope analysis

Rhenium-Os analysis was conducted at the Durham Geochemistry Centre at Durham University using standard procedures for organic-rich sedimentary rocks. Samples were visually inspected to avoid signs of weathering, veining, and diagenetic fracture fills, and then powdered and homogenized by hand in a porcelain mortar and pestle. Twenty to 40 grams of material from each sample were powdered, from which ~1 g was used for Re-Os isotope analysis. The Re-Os analysis utilizes carius tube digestion to homogenize sample and tracer solution (spike), then solvent extraction, microdistillation, and chromatography methods to isolate and purify the Re and Os fractions (Shirley and Walker, 1995; Cohen and Waters, 1996; Birck et al., 1997; Kendall et al., 2004; Selby and Creaser, 2003; Cumming et al., 2012). In brief, ~1g of sample, plus a known amount of spike solution (^{190}Os + ^{185}Re) together with 8 mL of Cr^{VI}–H_2SO_4 solution (used to limit the incorporation of detrital Re and Os) were digested in a sealed carius tube for 48 hours at 220°C (Kendall et al., 2004; Selby and Creaser, 2003). The Os was purified using the solvent extraction ($CHCl_3$), and Cr^{VI}–H_2SO_4 – HBr micro-distillation. Rhenium was isolated and further purified using NaOH-acetone solvent extraction and anion chromatography methods. The purified Re and Os fractions were loaded onto Ni and Pt filaments, respectively (Selby, 2007), with the isotopic measurements performed using a ThermoScientific TRITON mass spectrometer via static Faraday collection for Re and ion-counting using a secondary electron multiplier in peak-hopping mode for Os. Total procedural blanks during this study were 12.1 ± 0.36 pg and 0.07 ± 0.02 pg for Re and Os, respectively, with an average $^{187}Os/^{188}Os$ value of 0.21 ± 0.03 (n = 3). To monitor the long-

term reproducibility of mass spectrometer measurements two in-house Re and Os (DROsS) solution standards are analyzed, which yield an average $^{185}Re/^{187}Re$ and $^{187}Os/^{188}Os$ ratio of 0.59837 ± 0.0003 and 0.16089 ± 0.00056 (1 S.D., n = 5), respectively during this study.

Uncertainties for $^{187}Re/^{188}Os$ and $^{187}Os/^{188}Os$ were determined by full error propagation of uncertainties in Re and Os mass spectrometer measurements, blank abundances and isotopic compositions, spike calibrations and reproducibility of standard Re and Os isotopic values. The Re-Os isotopic data including 2σ calculated uncertainties for $^{187}Re/^{188}Os$ and $^{187}Os/^{188}Os$ and the associated error correlation function (rho) were regressed to yield a Re–Os date using *Isoplot V4.15* and the λ ^{187}Re constant of $1.666 \times 10^{-11}a^{-1}$ (Ludwig, 1980, 2008; Smoliar et al., 1996).

3.3 XRF spectroscopy

X-ray fluorescence spectroscopy was collected, using two Bruker Tracer III-SD XRF spectrometers equipped with Rh x-ray tubes, to determine bulk elemental concentrations. Measurements were collected on both cores every 1 cm in the R4 Zone oil shale bed (instrument T3S2798), and every 7.62 cm (3 inches) above and below (instrument T3S2470). The instruments interrogate the composition over an area of 3 mm by 3 mm. Samples were analyzed for 60 seconds at 15 kV and 25 μA (T3S2798) and 15 kV and 20 μA (T3S2470) with a He purge to measure Al, Ba, Ca, Cr, K, Mg, Mn, P, S, Si, Ti, and V. A second analysis was conducted for 60 seconds at 40 kV and 30 μA (T3S2798) and 40 kV and 40 μA (T3S2470) with a 12 mil Al + 1 mil Ti filter for As, Co, Cu, Fe, Ga, Mo, Nb, Ni, Pb, Rb, Se, Sr, Th, U, Y, Zn, and Zr. Instrument calibration (Spiegel, 2016; Brembs, 2017) followed the procedure of Rowe et al. (2012) using 41 mudrock samples with known elemental concentrations. Uncertainties, based on the analysis of standards and 100 replicated analyses of a single sample, are <0.5 wt. % (2σ) for the major elements Al, Ca, K, Mg, Si, and Ti, and <10 ppm (2σ) for the minor element Cr and Zr discussed below

(Supplemental Data). Measurements from both instruments were compared where they overlap and no systematic shifts were detected, thus the results were combined into a single dataset.

3.4 Total organic carbon content

The total organic carbon content (TOC) of 12 samples (Table 1) was measured at the USGS Petroleum Geochemistry Research Laboratory in Denver, Colorado using a LECO C744 Carbon Analyzer following the manufacturer's instructions. Samples were acidified with 6 M HCl and rinsed with deionized water prior to combustion to remove inorganic carbon (carbonate). Quality control materials including blanks, geochemical reference materials, and manufacturer's calibration standards were analyzed as part of the batch containing the samples. TOC uncertainty is 0.06 % (2σ) based on the analysis of 10 standards during the analytical period.

4. Results

4.1 Re and Os isotopes

Rhenium and Os concentrations range from 11.3 to 34.5 ppb and 106 to 213 ppt, respectively (Table 1). These are similar to concentrations reported from the underlying Douglas Creek Member and overlying Mahogany Zone in a nearby core in the eastern Uinta Basin (Cumming et al., 2012). Also similar are the $^{187}Re/^{188}Os$ values (~550 to 1050) that are positively correlated with $^{187}Os/^{188}Os$ compositions (~1.9 to 2.3). Linear regressions of $^{187}Re/^{188}Os$ and $^{187}Os/^{188}Os$ ratios of samples from the Skyline 16 and PR15-7c cores yield Model 3 age determinations of 47.4 ± 4.5 Ma (2σ, MSWD = 11.4; Os_i = 1.49 ± 0.06) and 51.7 ± 5.0 (2σ,

MSWD = 2.7; Os_i = 1.43 ± 0.08) Ma, respectively (Figs. 4A, B). Given the temporal equivalence of the two cores, the entire data set was regressed together and yields a Model 3 age of 48.3 ± 2.8 Ma (2σ, MSWD = 8.2), with an Os_i of 1.48 ± 0.04 (Fig. 4C).

An Os_i estimate for each sample (Table 1) was calculated using the ^{187}Re decay constant of 1.666 x 10^{-11} per year (Smoliar et al., 1996) and a depositional age of 49.54 Ma, which is the $^{40}Ar/^{39}Ar$ age of the Skyline ash (49.58 ± 0.32 Ma Smith and Carroll, 2015) minus the estimated temporal offset of -40,000 years (2 cycles). Analytical uncertainty was fully propagated using the square root of the sum of squares approach and includes the uncertainty of the measured $^{187}Re/^{188}Os$ and $^{187}Os/^{188}Os$ ratios and the 0.35% uncertainty of the ^{187}Re decay constant (Smoliar et al., 1996).

4.2 Major element geochemistry and TOC

Major element chemistry is relatively uniform in the R4 oil shale (Supplemental Data), while TOC ranges from 2.8 to 8.7 (Table 1). In general, Ca and Mg concentrations are consistently low in the oil shale and high in the underlying and overlying deposits where Si and Al concentrations are low (Fig. 2). This indicates that the oil shales are more siliciclastic-rich, and the shallower water facies are more calcareous (calcite and dolomite). The Si/Al ratio, a proxy for the bulk mineralogy of detrital sediments, is nearly constant in the oil shale (Fig. 2), as are the ratios of other detrital proxies such as Cr, K, Ti, and Zr to Al (Supplemental Data) suggesting a uniform detrital minerology throughout the sampled interval in both cores.

Cross plots of Os_i versus Ca, the Si/Al ratio, and TOC were constructed to investigate the relation between Re-Os isotope results and bulk rock elemental concentrations and organic matter content. These plots indicate that there is no correlation between these various data sets (Figs. 5A,

5B, & 5C). There is also no correlation between Re and Os concentrations and the Si/Al ratio, or between major element chemistry (Ca) and TOC (Figs. 5D, 5E, & 5F).

5. Discussion

5.1 Geochronology

All Re-Os ages, although imprecise (~6 to 10 %), are statistically indistinguishable from each other, from the $^{40}Ar/^{39}Ar$ sanidine age of the Skyline Ash, and from Re-Os ages reported for three other oil shale beds in the Green River Formation (Cumming et al., 2012). It is unlikely that the large age uncertainty is related to the $^{187}Re/^{188}Os$ range of ~500 observed in the sample set (Selby and Creaser, 2005; Kendall et al., 2009). If there is no inter-sample Os_i variability, a theoretical sample set with a $^{187}Re/^{188}Os$ range of 500, a depositional age of 50 Ma, and average analytical uncertainties based on the data reported here yields an isochron age with uncertainty of only 1.3 Myrs and $^{187}Os/^{188}Os$ intercept with uncertainty of only 0.01. These are both less than half the uncertainties reported above (Fig. 4C).

Error propagation was also investigated using the Monte Carlo approach of Li et al. (2018). In this technique a prescribed number of isochrons (10^6) are constructed from the input data and their corresponding probability density function (analytical uncertainty of $^{187}Re/^{188}Os$ and $^{187}Os/^{188}Os$ values, and their error correlation, *rho*). The age and Os_i estimate for each iteration are cross plotted yielding a probabilistic distribution that includes analytical uncertainty (Fig. 6). Model uncertainties, those attributed to the isochron linear regression, are also calculated (Li et al., 2018). Considering only analytical uncertainty, an age of 48.33 ± 0.95 Ma and an Os_i value of 1.48 ± 0.01 were calculated from the entire dataset (Fig. 6). Including both analytical and model uncertainty, collectively termed total uncertainty, an age of 48.33 ± 3.07 Ma and Os_i value of 1.48

± 0.04 are calculated. Uncertainties derived from the Monte Carlo approach are similar to those calculated using *Isoplot V4.15*. The Monte Carlo results suggest that model uncertainty accounts for about 70% of the age uncertainty and 75% of the Os_i uncertainty. Model uncertainties include the assumptions that all samples have nearly identical ages, the same initial $^{187}Os/^{188}Os$ composition, and that the Re-Os isotopic system was closed. Although open/closed system dynamics were not investigated here, previous studies have shown that the Re-Os isotopic system remains largely unaltered during thermal maturation of organic-rich mudstones and petroleum migration when there is a lack of hydrothermal activity (Rooney et al, 2012; and references therein). The assumption of a nearly identical age for all samples is robust as discussed above. The use of a Model 3 regression and a MSWD significantly greater than 1 in the *Isoplot* calculation; however, indicates that Os_i variability between samples is above the level of analytical uncertainty (Ludwig, 2008), violating the assumption for geochronology that all samples have an identical initial isotope composition. Although this puts a constraint on the ultimate resolution of age determinations, it suggests that the inter-sample Os_i variability is geologically significant.

5.2 Os_i stratigraphy

The calculated Os_i values for each sample in the two cores oscillate between 1.43 and 1.49, with changes in Os_i being penecontemporaneous (Table 1; Fig. 7). The Os_i values are within the range of $^{187}Os/^{188}Os$ values of average modern river water (~1.2-1.5; Lu et al., 2017). Recalculating Os_i using a depositional age of 49.525 Ma, the estimated top of the sampled interval, only changes the Os_i values in the third decimal place. Thus, the stratigraphic Os_i profile reported here is likely not an effect of varying depositional age.

Initial $^{187}Os/^{188}Os$ values increase across the upper Skyline ash, systematically decrease then increase above the ash, and finally decrease near the top of the R4 oil shale (Fig. 7). Volcanic

aerosols and erosion of ash from the landscape may provide temporally discreet contributions of non-radiogenic Os (~0.12-0.6) to basins with nearby volcanic centers (Lu et al., 2017); however, this does not appear to have occurred following deposition of the upper Skyline ash. Although the reported Os_i variability is just above analytical uncertainty, the similarity of the trend between the cores is striking and further supports the assertion that it represents a primary signal rather than analytical noise or an effect of diagenesis. Taken with the inability to obtain a Model 1 regression and a high MSWD (8.2), the Os_i profiles are interpreted as a record of changing $^{187}Os/^{188}Os$ composition of Lake Uinta water during deposition of the R4 oil shale. This can be explained by changes in the relative discharge of rivers or groundwater, the main sources of hydrogenous Os to lakes, with different Os isotopic compositions. The uniformity of detrital proxies in the R4 oil shale (Fig. 2; Supplemental Data), and lack of correlation with Os_i values (Fig. 5), suggests that there was not a contemporaneous change in sediment provenance; at least not one that is manifest in the major element geochemistry of the fine-grained sediments.

The $^{187}Os/^{188}Os$ value of surface and groundwater is controlled by the Os isotopic composition, Os content, and weatherability of bedrock and sediments in their drainage basins (Peucker-Ehrenbrink and Ravizza, 2000; Lu et al., 2017). Thus, modifications to the footprint or rocks exposed in the drainage basin, which are driven by climatic, tectonic, and geomorphic change, can explain the observed Os_i stratigraphy. This conclusion is similar to what was suggested for systematic $^{87}Sr/^{86}Sr$ variation through lake expansion-contraction cycles in the Green River Formation of Wyoming (Rhodes et al., 2002). There, $^{87}Sr/^{86}Sr$ values decreased during lake highstands which was attributed to increased drainage basin size, likely indicating a wetter climate that captured non-radiogenic runoff from Phanerozoic limestones. During lowstands the drainage basin was limited to the surrounding Precambrian-cored uplifts and exposed lake margin siliciclastic sediments, yielding more radiogenic water.

Similar stratigraphic Os_i variability to that reported above was documented in individual

lacustrine oil shale beds of the Douglas Creek Member (Os_i range of 1.30 to 1.47 over 1.2 meters of stratigraphic section) in the Uinta Basin (Cumming et al., 2012) and the Toarcian Da'anzhai Member (Os_i range of 1.23 to 1.31 over 0.42 meters of stratigraphic section) in the Sichuan Basin, China (Xu et al., 2017). However, neither of those studies compared results from two correlatable cores as is documented here. Cumming et al. (2012) argued against a diagenetic source of this variability. The results from the current study cast further doubt on a diagenetic interpretation. Thus, our findings provide confidence that the Os_i variability reported in the Douglas Creek and Da'anzhai members is geologically significant, indicating changes in the $^{187}Os/^{188}Os$ composition of lake waters through time.

5.3 Os_i sensitivity

To investigate the magnitude of change in the Os isotopic abundance of water entering Lake Uinta need to match the Os_i range documented here, a simple two-component steady-state mixing model was used (cf., Faure, 1986). Unfortunately, the Os isotopic composition of bedrock surrounding the Uinta Basin is not known; however, it does contain Precambrian formations that commonly yield highly radiogenic water (~2-4), Phanerozoic sedimentary rocks which produce moderately radiogenic water (~1-2), and volcanic terranes that yield relatively non-radiogenic water (<1) (Peucker-Ehrenbrink and Ravizza, 1996; Peucker-Ehrenbrink and Ravizza, 2000; Lu et al., 2017). Thus, global averages were used to constrain the endmembers of six isotopic mixing models (Table 2). An endmember with an $^{187}Os/^{188}Os$ ratio of 1.0 was used to represent the contribution from Phanerozoic sedimentary rocks. Two radiogenic endmembers with $^{187}Os/^{188}Os$ ratios of 2.0 and 4.0 were used to represent the contribution from Precambrian bedrock. All Os_i values reported in this study lie between these endmembers. One set of models assumed that both endmembers have the same Os concentration of 5 pg/kg (Table 2; Fig. 8A). A second set of models

tested the effects of one endmember with 5 pg/kg of Os and the other with a concentration of 50 pg/kg (Table 2; Fig. 8B), roughly the range of Os concentrations in modern river water (Peucker-Ehrenbrink and Ravizza, 2000; Lu et al., 2017). All models indicate that the range of Os_i values measured in the R4 oil shale (1.43 to 1.49) can be explained by less than a 6% change in the relative contribution of water from non-radiogenic and radiogenic endmembers (Table 2). This amount of variation in water input, and related drainage basin reorganization, is not difficult to imagine for a lacustrine setting. More importantly these results highlight the extreme sensitivity of Os isotopes as a tracer of lake water provenance, namely that only a very minor change in the contribution of water from different endmembers yields measurable Os_i variability in lacustrine oil shales at or just above the level of analytical uncertainty.

It should be noted that these simple models assume Lake Uinta reached a steady-state Os isotopic abundance equal to the mixture of the two endmembers geologically instantaneously compared to the sample interval of about 1,500 years. A flux model or mass balance approach (cf. Doebbert et al., 2014) which includes the buffering capacity of the Os reservoir in the lake and Os deposition should be explored. Analysis of bedrock samples and modern rivers surrounding the Uinta Basin would also aid in constraining this these models.

Using a depositional period of 15,000 years for the sampled interval and the constant sedimentation rate estimated above, the rate of change between Os_i minima (1.43) and maxima (1.49) is about 0.01 per kiloyear. This is two orders of magnitude faster than what was reported from marine metalliferous pelagic clay in the North Pacific near the K-T boundary, caused by an instantaneous influx of meteoritic Os (Ravizza, 2007). The rapid change documented in this study indicates that Os residence times in lakes are likely less than in the ocean, similar to what has been modeled for Sr (Doebbert et al., 2014).

6. Conclusions

Samples of the same oil shale bed of the Green River Formation from two cores, separated by 16 km in the eastern Uinta Basin yield a depositional age of 48.3 ± 2.8 Ma which is indistinguishable from the nearby 49.58 ± 0.32 Ma $^{40}Ar/^{39}Ar$ age determination of the Skyline ash (Smith and Carroll, 2015). However, a high MSWD, use of a Model 3 age, and the similarity in Os_i stratigraphy between the two cores suggests that the observed temporal Os_i variability is geologically significant, recording changing lake water chemistry. Simple two-component steady-state mixing models indicate that the Os_i range documented here, which is at or just above the level of analytical uncertainty, can be explained by a very minor change (<6%) in the source of water entering Lake Uinta. This Os_i variability appears to have occurred at a rate that is 100 times quicker than has been documented in the marine setting. Together, the results of this study show that Os isotope stratigraphy from lacustrine organic-rich sedimentary rocks has the potential to provide new, high resolution, evidence of drainage basin and landscape evolution which are driven by climatic, tectonic, and geomorphic processes.

Acknowledgments

Acknowledgment is made to the Donors of the American Chemical Society Petroleum Research Fund for support of this research (to JTP). Additional support was provided (to RB) by the SEPM Society for Sedimentary Geology and the Utah Geological Survey. We thank Michael Vanden Berg, Lauren Birgenheier, and the staff of the Utah Core Research Center at the Utah Geological Survey for valuable geologic discussions, logistical support, and access to core samples. We thank Justin Birdwell and the staff of the USGS Geochemistry laboratory for TOC analysis. DS is thankful for the ongoing support from Antonia Hofmann, Geoff Nowell, and Chris Ottley. DS acknowledges the Total endowment Fund and CUG Wuhan Dida Scholarship. Finally,

we thank the anonymous reviews who provided constructive comments to early versions of this manuscript.

References

Aswasereelert, W., Meyers, S.R., Carroll, A.R., Peters, S.E., Smith, M.E., Feigl, K.L., 2013, Basin-scale cyclostratigraphy of the Green River Formation, Wyoming: Geological Society of America Bulletin, v. 125, p. 216–228.

Baddouh, M., Carroll, A.R., Meyers, S.R., Beard, B.L., and Johnson, C.M., 2017, Chronostratigraphic correlation of lacustrine deposits using $^{87}Sr/^{86}Sr$ ratios, Eocene Green River Formation, Wyoming, U.S.A: Journal of Sedimentary Research, v. 87, p. 406-423.

Berman, A. 2008, Three super-giant fields discovered in Brazil's Santos Basin: World Oil, February 2008, p. 23–24.

Birgenheier, L.P., and Vanden Berg, M.D., 2011, Core-based integrated sedimentologic, stratigraphic, and geochemical analysis of the oil shale bearing Green River Formation, Uinta Basin, Utah: Topical Report submitted to the U.S. Department of Energy, National Energy Technology Laboratory, DOE Award No. DE-FE0001243, Salt Lake City, Utah, University of Utah, Institute for Clean and Secure Energy.

Birck, J.L., Roy-Barman, M., and Capmas, F., 1997, Re-Os isotopic measurements at the femtomole level in natural samples: Geostandards Newsletter, v. 20, p. 19-27.

Brembs, R.G, 2017, Cyclostratigraphy and chemostratigraphy in the Parachute Creek Member of the Eocene Green River Formation, eastern Uinta Basin, Utah [MS Thesis]: Binghamton University, State University of New York, Binghamton, New York, 246 p.

Chaboureau, A.C., Guillocheau, F., Robin, C., Rohais, S., Moulin, M., and Aslanian, D., 2013, Paleogeographic evolution of the central segment of the South Atlantic during Early Cretaceous times; paleotopographic and geodynamic implications: Tectonophysics, v. 604, p.

191-223.

Cohen, A.S., Coe, A.L., Bartlett, J.M., and Hawkesworth, C.J., 1999, Precise Re-Os ages of organic-rich mud rocks and the Os isotope composition of Jurassic seawater: Earth and Planetary Science Letters, v. 167, p. 159-173.

Cohen, A.S., and Waters, F.G., 1996, Separation of osmium from geological materials by solvent extraction for analysis by thermal ionization mass spectrometry: Analytica Chimica Acta, v. 332, p. 269-275.

Creaser, R., Szatmari, P., Milani, E.J., 2008, Extending Re-Os shale geochronology to lacustrine depositional systems: a case study from the major hydrocarbon source rocks of the Brazilian Mesozoic marginal basins: International Geological Congress, 33rd, Oslo, Norway, Abstracts.

Cumming, V.M., Selby, D., and Lillis, P.G., 2012, Re–Os geochronology of the lacustrine Green River Formation: Insights into direct depositional dating of lacustrine successions, Re-Os systematics and paleocontinental weathering: Earth and Planetary Science Letters, v. 359-360, p. 194-205.

Demaison, G., and Moore, G.T., 1980, Anoxic environments and oil source bed genesis: American Association of Petroleum Geologists, Bulletin, v. 64, p. 1179-1209.

de Wit, M.J., Stankiewicz, J., and Reeves, C., 2008, Restoring Pan-African/Brasiliano connections; more Gondwana control, less trans-Atlantic corruption, *in* Pankhurst, R.J., Trouw, R.A.J, Brito Neves, B.B., and de Wit, M. J., eds, West Gondwana; pre-Cenozoic correlations across the South Atlantic region: Geological Society Special Publications, 2008, v. 294, p. 399-412.

Dickinson, W.R., Klute, M.A., Hayes, M.J., Janecke, S.U., Lundin, E.R., McKittrick, M.A., and Olivares, M.D., 1988, Paleogeographic and paleotectonic setting of Laramide sedimentary basins in the central Rocky Mountain region: Geological Society of America Bulletin, v. 100, p. 1023-1039.

Doebbert, A.C., Johnson, C., Carroll, A.R., Beard, B. Pietras, J.T, Rhodes Carson, M., Norsted, B., and Throckmorton, A., 2014, Controls on Sr isotopic evolution in lacustrine systems: Eocene Green River Formation, Wyoming: Chemical Geology, v. 380, p. 172-189.

Du Vivier, A.D.C., Selby, D., Sageman, B.B., Jarvis, I., Gröcke, D.R., and Voigt, S., 2014, Marine $^{187}Os/^{188}Os$ isotope stratigraphy reveals the interaction of volcanism and ocean circulation during Oceanic Anoxic Event 2: Earth and Planetary Science Letters, v. 389, p. 22-33.

Du Vivier, A.D.C., Selby, D., Condon, D.J., Takashima, R., and Nishi, H., 2015, Pacific $^{187}Os/^{188}Os$ isotope chemistry and U–Pb geochronology: Synchroneity of global Os isotope change across OAE 2: Earth and Planetary Science Letters, v. 428, p. 204-216.

Faure, G., 1986, Principles of isotope geology (2nd ed.): Wiley, New York, 589p.

Gierlowski, E.H., and Kelts, K.R., 2000, Lake basins through space and time: American Association of Petroleum Geologists Studies in Geology 46, Tulsa, Oklahoma, 648 p.

Gierlowski-Kordesch, E.H., Jacobson, A.D., Blum, J.D., and Valero Garćes, B.L., 2008, Watershed reconstruction of a Paleocene–Eocene lake basin using Sr isotopes in carbonate rocks: Geological Society of America Bulletin, v. 120, p. 85-95.

Hayden, F. V., 1869, Preliminary field report of the United States Geological Survey of Colorado and New Mexico: Washington, Government Printing Office, 155p.

Jones, C.E., and Jenkyns, H.C., 2001, Seawater strontium isotopes, oceanic anoxic events, and seafloor hydrothermal activity in the Jurassic and Cretaceous: American Journal of Science, v. 301, p. 112-149.

Johnson, R.C., 1989, Detailed cross sections correlating upper Cretaceous and lower Tertiary rocks between the Uinta Basin of Eastern Utah and Western Colorado and the Piceance Basin of Western Colorado: U.S. Geological Survey Miscellaneous Investigations Map I-1974, 2 large sheets.

Johnson, S.Y., 1992, Phanerozoic evolution of sedimentary basins in the Uinta-Piceance Basin region, Northwestern Colorado and Northwestern Utah: U.S. Geological Survey Bulletin 1787-FF, 38 p.

Katz, B.J, 1990, Lacustrine basin exploration, American Association of Petroleum Geologists Memoir 50, Tulsa, Oklahoma, 340 p.

Kendall, B.S., Creaser, R.A., Ross, G.M., Selby, D., 2004, Constraints on the timing of Marinoan "Snowball Earth" glaciation by ^{187}Re-^{187}Os dating of a Neoproterozoic, post-glacial black shale in Western Canada. Earth and Planetary Science Letters 222, 729-740.

Kendall, B., Creaser, R.A., Selby, D., 2009, ^{187}Re-^{187}Os geochronology of Precambrian organic-rich sedimentary rocks: Geological Society Special Publications 326, London, p.85-107.

Li, Y., Zhang, S., Hobbs, R., Caiado, C., Sproson, A.D., Selby, D., Rooney, A.D., 2018, Monte Carlo sampling for error propagation in linear regression and applications in isochron geochronology: Science Bulletin, v. 64, p. 189-197.

Lu, X., Kendall, B., Stein, H.J., and Hannah, J.L., 2017, Temporal record of osmium concentrations and ^{187}Os/^{188}Os in organic-rich mudrocks: Implications for the osmium geochemical cycle and the use of osmium as a paleoceanographic tracer: Geochimica et Cosmochimica Acta, v. 216, p. 221-241.

Ludington, S., Moring, B.C., Miller, R.J., Stone, P.A., Bookstrom, A.A., Bedford, R.T., Evans, J.G., Haxel, G.A., Nutt, C.J., Flyn, K.S., and Hopkins, M.J., 2005, Preliminary integrated geologic map databases for the United States - western states: California, Nevada, Arizona, Washington, Oregon, Idaho, and Utah: U.S. Geological Survey Open-File Report 2005-1305.

Ludwig, K.R., 1980, Calculation of uncertainties of U-Pb isotope data. Earth and Planetary Science Letters 46, 212-220.

Ludwig, K.R., 2008, Isoplot version 3.70: A geochronological toolkit for microsoft Excel: Berkeley Geochronology Center Special Publication No. 4, 76 p.

Machlus, M.L., Ramezani, J., Bowring, S.A., Hemming, S.R., Tsukui, K., and Clyde, W.C., 2015, A strategy for cross-calibrating U-Pb chronology and astrochronology of sedimentary sequences: An example from the Green River Formation, Wyoming, USA: Earth and Planetary Science Letters, v. 413, p. 70-78.

McArthur, J.M., Howarth, R.J., and Shields, G.A., 2012, Strontium isotope stratigraphy, *in* Grandstein, F.M., Ogg, J.G, Schmitz, M., and Ogg, G., eds., The Geological Time Scale 2012: Elsevier, Amsterdam, p. 127-144.

Meyers, S.R., 2008, Resolving Milankovitchian controversies: The Triassic Latemar Limestone and the Eocene Green River Formation: Geology, v. 36, p. 319-322.

Moulin, M., Aslanian, D., and Unternehr, P., 2010, A new starting point for the South and Equatorial Atlantic Ocean: Earth-Science Reviews, v. 98, p. 1-37.

Pietras, J.T., and Carroll, A.R., 2003, Different Lake Types, Same Organic Matter Accumulation Rate: Implications for Carbon Burial in the Eocene Green River Formation: GSA Abstracts with Programs, v. 35, p. 104.

Pietras, J.T., Carroll, A.R., Singer, B.S., and Smith, M.E., 2003, 10,000 yr depositional cyclicity in the early Eocene: Stratigraphic and $^{40}Ar/^{39}Ar$ evidence from the lacustrine Green River Formation: Geology, v. 31, p. 593-596.

Peucker-Ehrenbrink, B., Jahn, B., 2001, Rhenium–osmium isotope systematics and platinum group element concentrations: Loess and the upper continental crust: Geochemistry, Geophysics, Geosystems, v. 2, p. 1061-1083.

Peucker-Ehrenbirnk, B., and Ravizza, G., 1996, Continental runoff of osmium into the Baltic Sea: Geology, v. 24, p. 327-330.

Peucker-Ehrenbirnk, B., and Ravizza, G., 2000, The marine osmium isotope record: Terra Nova, v. 12, p. 205-219.

Peucker-Ehrenbirnk, B., and Ravizza, G., 2012, Osmium isotope stratigraphy, *in* Grandstein, F.M., Ogg, J.G, Schmitz, M., and Ogg, G., eds., The Geological Time Scale 2012: Elsevier, Amsterdam, p. 145-166.

Poirier, A., and C. Hillaire-Marcel, 2011, Improved Os-isotope stratigraphy of the Arctic Ocean: Geophysical Research Letters, v. 38, L14607, 6p.

Quirk, D.G., Hertle, M., Jeppesen, J.W., Raven, M., Mohriak, W.U., Kann, D.J., Norgaard, M., Howe, M.J., Hsu, D., Coffey, B., and Mendes, M.P., 2013, Rifting, subsidence and continental break-up above a mantle plume in the central South Atlantic, *in* Mohriak, W.U., Danforth, A., Post, P.J., Brown, D.E., Tari, G.C., Nemčok, M., and Sinha, S.T., eds., Conjugate divergent margins: Geological Society Special Publications, v. 369.

Rangel, H.D., and Carminatti, M., 2000, Rift lake stratigraphy of the Lagoa Feia Formation, Campos Basin, Brazil, *in* Gierlowski-Kordesch, E.H, and Kelts, K.R, eds., Lake basins through space and time: American Association of Petroleum Geologists Studies in Geology 46, p. 225-244.

Ravizza, G.E., 2007, Reconstructing the marine $^{187}Os/^{188}Os$ record and the particulate flux of meteoritic osmium during the late Cretaceous: Geochimica et Cosmochimica Acta, v. 71, p. 1355-1369.

Ravizza, G., and Turekian, K.K., 1989, Application of the ^{187}Re-^{187}Os system to black shale geochronometry: Geochimica et Cosmochimica Acta, v. 53, p. 3257-3262.

Rhodes, M.K., Carroll, A.R., Pietras, J.T., Beard, B.L., and Johnson, C.M., 2002, Strontium isotope record of paleohydrology and continental weathering, Eocene Green River Formation, Wyoming: Geology v. 30, p. 167-170.

Rooney, A.D, Selby, D., Lewan, M.D., Lillis, P.G., and Houzay, J-P., 2012, Evaluating Re-Os systematics in organic-rich sedimentary rocks in response to petroleum generation using hydrous pyrolysis experiments: Geochimica et Cosmochimica Acta, v. 77, p. 275-29.

Rooney, A.B., Selby, D.S., Lloyd, J.M., Roberts, D.H., Lueckge, A., Sageman, B.B., and Prouty, N.G., 2016, Tracking millennial-scale Holocene glacial advance and retreat using osmium isotopes; insights from the Greenland ice sheet: Quaternary Science Reviews, v. 138, p. 49-61.

Rowe, H., Hughes, N., and Robinson, K., 2012, The quantification and application of handheld energy-dispersive x-ray fluorescence (ED-XRF) in mudrock chemostratigraphy and geochemistry: Chemical Geology, v. 324, p. 122-131.

Selby, D., 2007, Direct rhenium-osmium age of the Oxfordian-Kimmeridgian boundary, Staffin bay, Isle of Skye, UK, and the late Jurassic timescale: Norwegian Journal of Geology, v. 87, p. 291–300.

Selby, D., Creaser, R.A., 2003, Re-Os geochronology of organic rich sediments: an evaluation of organic matter analysis methods: Chemical Geology, v. 200, p. 225-240.

Selby, D., Creaser, R.A., 2005, Direct radiometric dating of the Devonian-Mississippian time-scale boundary using the Re-Os black shale geochronometer: Geology, v. 33, p. 545-548.

Shirey, S.B., and Walker R.J., 1995, Carius tube digestion for low-blank Rhenium-Osmium analysis: Analytical Chemistry, v. 67, p. 2136-2141.

Smith, M.E., Singer, B., and Carroll, A., 2003, $^{40}Ar/^{39}Ar$ geochronology of the Eocene Green River Formation, Wyoming: Geological Society of America Bulletin, v. 115, p. 549-565.

Smith, M.E., Carroll, A.R., and Singer, B.S., 2008, Synoptic reconstruction of a major ancient lake system: Eocene Green River Formation, western United States: Geological Society of America Bulletin, v. 120, p. 54-84.

Smith, M.E., and Carroll A.R., 2015, Introduction to the Green River Formation, *in* Smith, M.E., and Carroll A.R., eds., Stratigraphy and paleolimnology of the Green River Formation, Western USA: Springer, Syntheses in Limnogeology 1, p. 1-12.

Smoliar M.I., Walker R.J., and Morgan J.W., 1996, Re-Os isotope constraints on the age of Group IIA, IIIA, IVA, and IVB iron meteorites: Science, v. 271, p. 1099–1102.

Spiegel, E.B., 2016, Chemostratigraphy of the Trenton Group and Utica Shale using XRF, XRD, Gamma Ray, and FTIR spectroscopy in the Mohawk Valley of Central New York [MS Thesis]: Binghamton University, State University of New York, Binghamton, New York, 178 p.

Stoeser, D.B., Green, G.N., Morath, L.C., Heran, D.W., Wilson, A.B., Moore, D.W., and Van Gosen, B.S, 2005, Preliminary integrated geologic map databases for the United States - Central states: Montana, Wyoming, Colorado, New Mexico, North Dakota, South Dakota, Nebraska, Kansas, Oklahoma, Texas, Iowa, Missouri, Arkansas, and Louisiana: U.S. Geological Survey Open-File Report 2005-1351.

Xu, W., Ruhl, M., Jenkyns, H.C., Hesselbo, S.P., Riding, J.B., Selby, D., Naafs, B.D.A., Weijers, J.W.H., Pancost, R.D., Tegelaar, E.W., and Idiz, E.F., 2017, Carbon sequestration in an expanded lake system during the Toarcian oceanic anoxic event; Nature Geoscience, v. 10, p. 129–134

Zaiss, J., Ravizza, G., Goderis, S., Sauvage, J., Claeys, P., and Johnson, K., 2014, A complete Os excursion across a terrestrial Cretaceous-Paleogene boundary at the West Bijou Site, Colorado, with evidence for recent open system behavior: Chemical Geology, v. 385, p. 7-16.

FIGURE CAPTIONS

Fig. 1. A) Generalized stratigraphic columns for the Skyline 16 and PR15-7c cores highlighting the position of the R4 oil shale, Skyline ash, and organic-rich (R) and organic-lean (L) zones in the lower Parachute Creek Member of the Green River Formation. Modified from Birgenheier and Vanden Berg (2011) and Brembs (2017). B) Map showing the location of the Skyline 16 and PR15-7c cores in the eastern Uinta Basin, and the general bedrock lithology surrounding the basin.

Sevier FTB - Sevier fold and thrust belt. Modified from Ludington et al. (2005) and Stoeser et al. (2005).

Fig. 2. Correlation of the studied lake expansion-contraction cycle between the Skyline 16 and PR15-7c cores showing the Ca, Mg, Si, and Al concentrations and the Si/Al ratio.

Fig. 3. Calculation of the depositional period of the total sampled interval and individual samples in the Skyline 16 core.

Fig. 4. A) Re-Os isochron plot of 12 samples from the R4 oil shale in the Skyline 16 core. B) Re-Os isochron plot of 7 samples from the R4 oil shale in the PR15-7c core. C) Re-Os isochron plot of all 19 samples from the R4 oil shale in both cores.

Fig. 5. Correlation of Re-Os results, XRF elemental concentrations, and TOC of samples from the Skyline 16 and PR15-7c cores. A) Os_i vs. Ca (wt.%), B) Os_i vs. Si/Al, C) Os_i vs. TOC, D) Re (ppb) vs Si/Al, E) Os (ppt) vs. Si/Al, and D) Ca (wt.%) vs. TOC. Error bars represent 2σ uncertainty, and those not shown are less than the size of the marker. Values are listed in Table 1 and in the Supplemental Data.

Fig. 6. Distribution of age and Os_i estimates based on the Monte Carlo approach. Inset shows total uncertainty at the 2σ level and the contribution to the total from analytical uncertainty. Analytical uncertainty accounts for 41% of the total. Age uncertainties include the uncertainty on the decay constant. Excluding decay constant uncertainty from the Monte Carlo calculation results in only a very small reduction in age uncertainty (≤ 2%).

Fig. 7. Chronostratigraphic correlation of Os_i values between the Skyline 16 and PR15-7c cores.

Fig. 8. Results of simple two-component steady-state mixing models between non-radiogenic and radiogenic water endmembers. See Table 2 for input parameters.

Declaration of competing interest

The authors declare that they have no known competing financial interests or personal relationships that could have appeared to influence the work reported in this paper.

TABLE 1. Re-Os ISOTOPE DATA

Sample Name	Depth (m)	Re (ppb)	±	Os (ppt)	±	^{192}Os (ppt)	±	^{187}Re/^{188}Os	±	^{187}Os/^{188}Os	±	rho[a]	% Re blank	% ^{187}Os blank	% ^{188}Os blank	Os_i[b]	±	TOC[c]
PR15-7c																		
PR1	16.50	35.48	0.09	21.8	1.0	68.4	0.3	1031.6	4.9	2.303	0.013	0.615	0.07	0.01	0.12	1.45	0.014	
PR2	16.65	25.75	0.06	15.9	0.8	50.8	0.2	1009.4	4.9	2.304	0.013	0.632	0.09	0.02	0.16	1.47	0.014	
PR3	16.60	24.30	0.06	14.9	0.8	46.1	0.2	1048.5	5.2	2.337	0.014	0.636	0.10	0.02	0.17	1.47	0.015	6.17
PR4	16.65	23.04	0.06	16.9	0.8	53.6	0.2	853.7	4.2	2.165	0.013	0.627	0.10	0.02	0.15	1.46	0.013	
PR5	16.68	28.01	0.07	19.1	1.0	63.0	0.3	884.8	4.7	2.204	0.013	0.588	0.09	0.01	0.13	1.47	0.016	
PR6	16.75	19.05	0.05	13.0	0.7	44.5	0.2	855.9	4.3	2.162	0.013	0.626	0.13	0.02	0.18	1.46	0.018	4.97
PR7	16.80	18.03	0.04	15.0	0.8	49.8	0.2	720.4	3.7	2.045	0.013	0.638	0.13	0.02	0.16	1.45	0.013	
Skyline 16																		
SL1	26.97	25.28	0.06	15.8	0.8	51.2	0.2	982.3	5.1	2.247	0.013	0.631	0.09	0.02	0.16	1.44	0.014	6.45
SL2	26.98	25.05	0.06	15.0	0.8	48.8	0.2	1041.7	5.4	2.311	0.013	0.632	0.09	0.02	0.16	1.45	0.014	5.63
SL3	26.98	20.30	0.05	14.0	0.7	46.2	0.2	881.1	4.6	2.218	0.013	0.637	0.12	0.02	0.17	1.49	0.013	5.01
SL4	26.99	19.54	0.05	14.0	0.7	47.5	0.2	819.4	4.2	2.165	0.012	0.635	0.12	0.02	0.17	1.49	0.012	5.26
SL5	26.99	15.13	0.04	13.0	0.7	44.1	0.2	684.8	3.6	2.035	0.013	0.645	0.16	0.02	0.18	1.47	0.013	
SL6	27.03	11.27	0.03	11.0	0.6	37.7	0.2	594.0	3.1	1.956	0.013	0.655	0.21	0.03	0.21	1.47	0.013	8.65
SL7	27.08	13.39	0.03	13.0	0.7	46.3	0.2	575.1	3.0	1.948	0.012	0.642	0.18	0.02	0.17	1.47	0.012	3.65
SL8	27.13	10.34	0.03	10.0	0.6	34.7	0.2	668.4	3.4	2.036	0.013	0.637	0.13	0.02	0.15	1.48	0.013	2.80
SL9	27.15	10.16	0.03	10.0	0.6	34.7	0.2	866.6	4.4	2.149	0.013	0.661	0.16	0.03	0.23	1.44	0.013	

	8	0	4	1	6		2		7		4	9				3	5	
	27	12	0.	12	0		0		3		0.	0.				1.	0.	
	0.2	.7	0	9.	.	43	.		.		01	64	0.	0.0	0.1	4	01	4.
SL10	3	1	3	4	7	.2	2	585.0	0	1.939	2	8	19	2	9	6	2	18
	27	13	0.	14	0		0		2		0.					1.	0.	
	0.2	.3	0	4.	.	48	.		.		01	0.	0.	0.0	0.1	4	01	5.
SL11	8	8	3	4	8	.3	2	551.1	9	1.918	2	62	18	2	7	6	2	98
	27	19	0.	15	0		0		3		0.	0.				1.	0.	
	0.3	.1	0	1.	.	49	.		.		01	64	0.	0.0	0.1	4	01	6.
SL12	3	5	5	6	8	.8	2	765.8	9	2.107	3	1	13	2	6	7	3	05

All uncertainties are reported at 2σ.

[a]rho is the associated error correlation at 2σ (Ludwig, 1980).

[b]Os_i is the initial $^{187}Os/^{188}Os$ isotopic ratio calculated at 49.54 Ma.

[c]TOC uncertainty is 0.06 (2σ) based on analysis of 10 standards during the analytical period.

TABLE 2. MIXING MODEL INPUTS AND RESULTS

Model	non-radiogenic endmember		radiogenic endmember		% change
	Os (pg/kg)	$^{187}Os/^{188}Os$	Os (pg/kg)	$^{187}Os/^{188}Os$	required
A1	5	1	5	2	6
A2	5	1	5	4	2
B1	50	1	5	2	3
B2	5	1	50	2	2
B3	50	1	5	4	3
B4	5	1	50	4	1

Highlights:

- Os isotope stratigraphy is a sensitive tracer in lacustrine deposits
- Os isotope profiles are consistent between correlative oil shale beds
- Re-Os geochronology of lacustrine oil shales match volcanic tuff ages

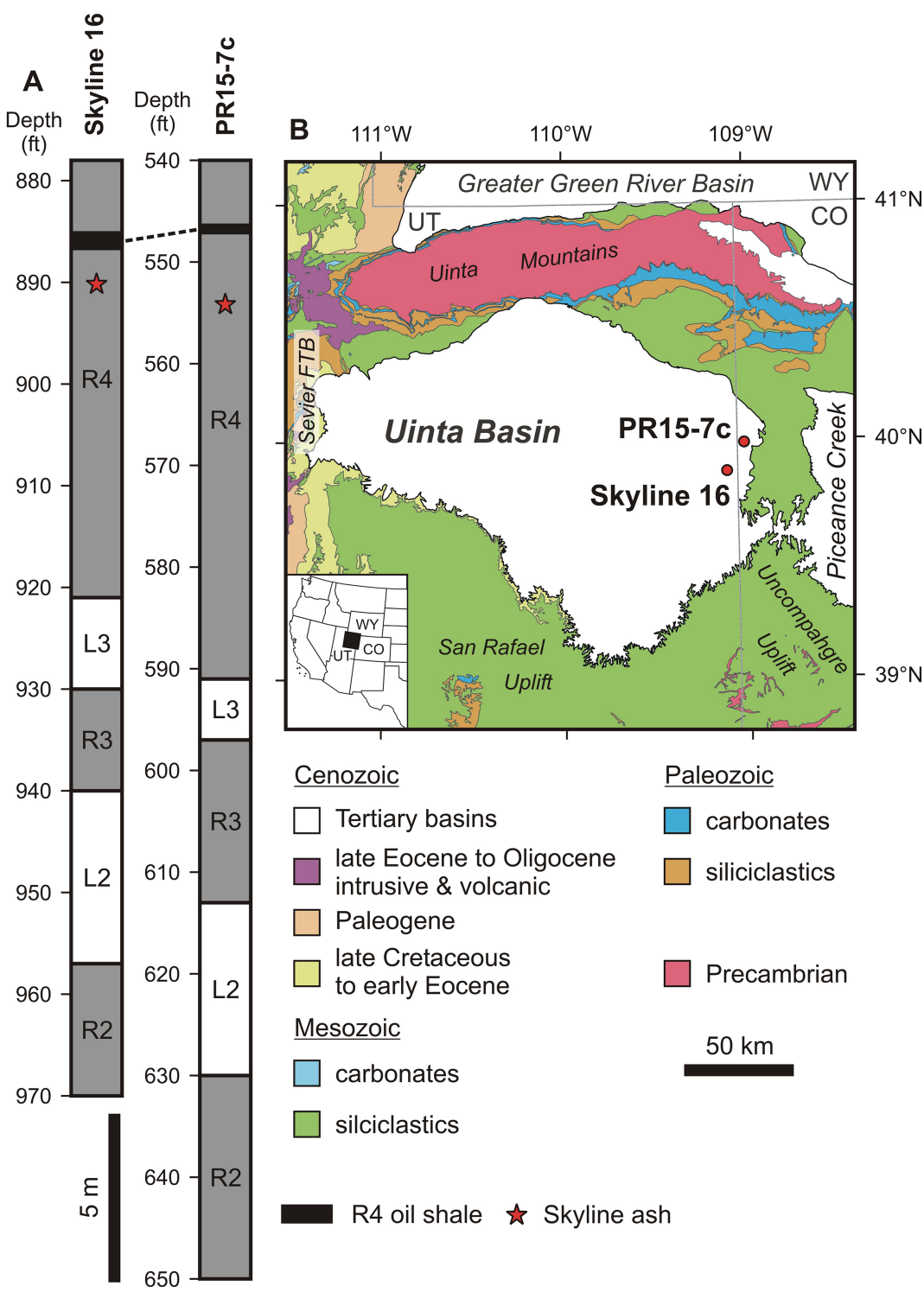
A
Depth (ft)
Skyline 16
Depth (ft)
PR15-7c
880
890
900
910
920
930
940
950
960
970
540
550
560
570
580
590
600
610
620
630
640
650
R4
L3
R3
L2
R2
5 m
B
111°W
110°W
109°W
41°N
40°N
39°N
Greater Green River Basin
WY
CO
UT
Uinta Mountains
Sevier FTB
Uinta Basin
PR15-7c
Skyline 16
Piceance Creek
Uncompahgre Uplift
San Rafael Uplift
Cenozoic
Tertiary basins
late Eocene to Oligocene intrusive & volcanic
Paleogene
late Cretaceous to early Eocene
Mesozoic
carbonates
silciclastics
Paleozoic
carbonates
siliciclastics
Precambrian
50 km
R4 oil shale
Skyline ash

Figure 1

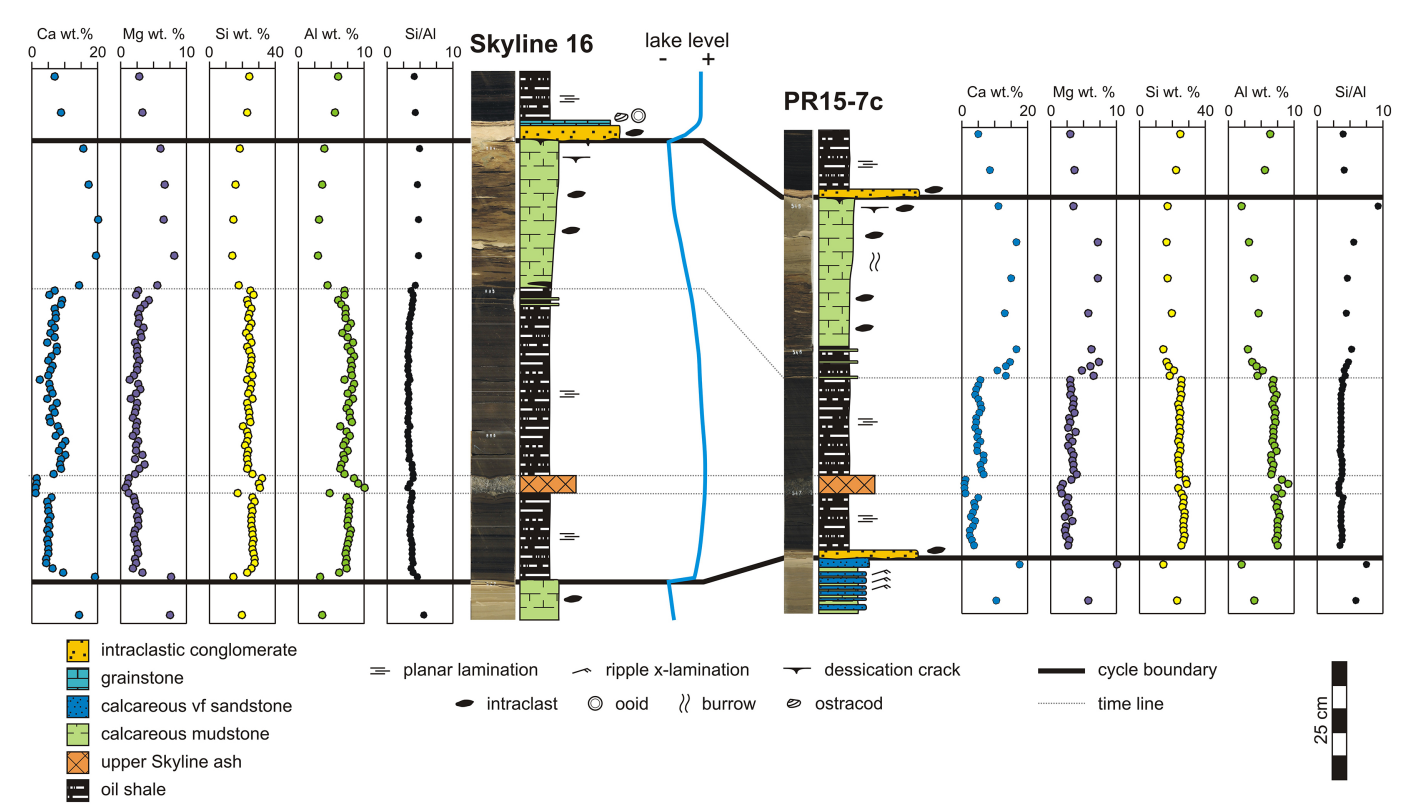
Ca wt.%
0
20
Mg wt. %
0
10
Si wt. %
0
40
Al wt. %
0
10
Si/Al
0
10
Skyline 16
lake level
-
+
PR15-7c
Ca wt.%
0
20
Mg wt. %
0
10
Si wt. %
0
40
Al wt. %
0
10
Si/Al
0
10
intraclastic conglomerate
grainstone
calcareous vf sandstone
calcareous mudstone
upper Skyline ash
oil shale
planar lamination
ripple x-lamination
dessication crack
intraclast
ooid
burrow
ostracod
cycle boundary
time line
25 cm

Figure 2

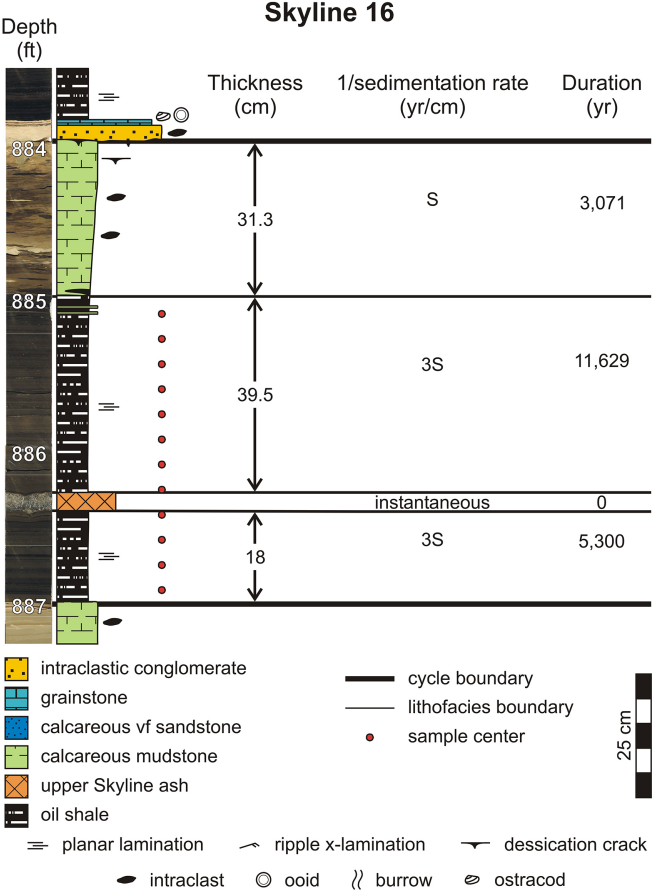

Calculations

(thickness of oil shale * 3S) + (thickness of other facies * S) = 20,000 years

(18 + 39.5 cm * 3S) + (31.3 cm * S) = 20,000 years

203.8 * S = 20,000 years

S = 98.14 years/cm

sampled interval = 52.15 cm * 3S = 15,350 years

individual sample = 5 cm * 3S = 1,472 years

Figure 3

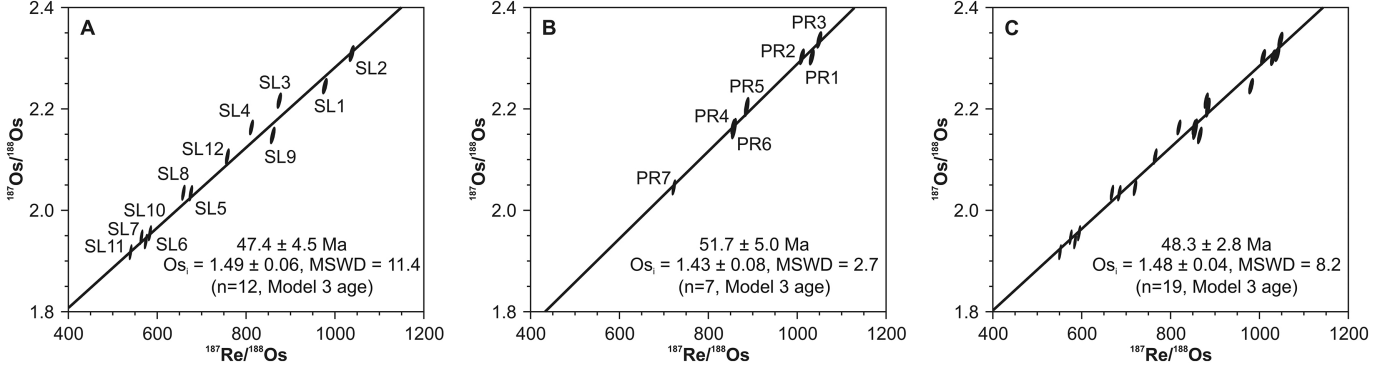
A
SL2
SL3
SL1
SL4
SL12
SL9
SL8
SL5
SL10
SL7
SL11
SL6
47.4 ± 4.5 Ma
Os$_i$ = 1.49 ± 0.06, MSWD = 11.4
(n=12, Model 3 age)
B
PR3
PR2
PR1
PR5
PR4
PR6
PR7
51.7 ± 5.0 Ma
Os$_i$ = 1.43 ± 0.08, MSWD = 2.7
(n=7, Model 3 age)
C
48.3 ± 2.8 Ma
Os$_i$ = 1.48 ± 0.04, MSWD = 8.2
(n=19, Model 3 age)
^{187}Os/^{188}Os
^{187}Re/^{188}Os
2.4
2.2
2.0
1.8
400
600
800
1000
1200

Figure 4

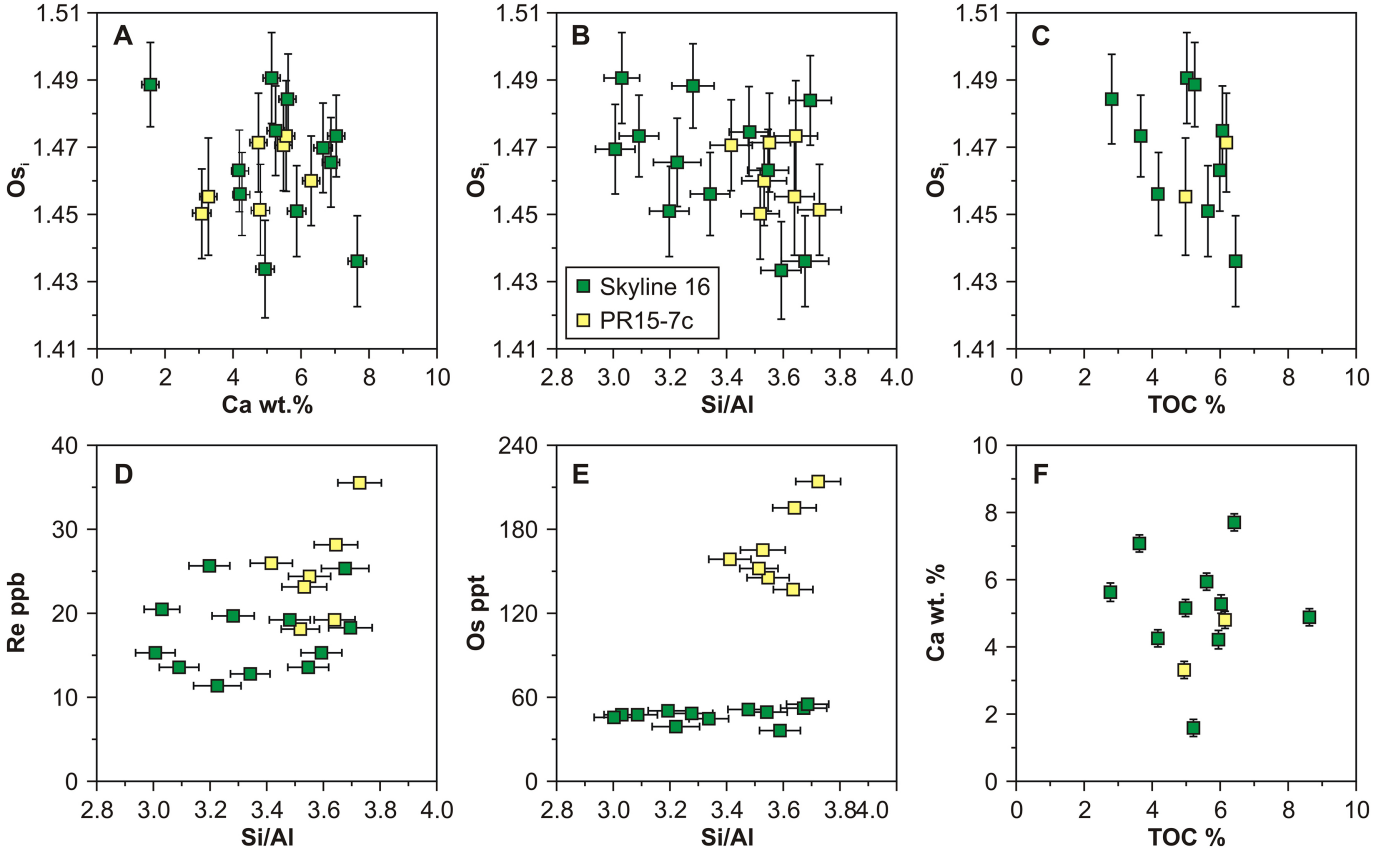

Figure 5

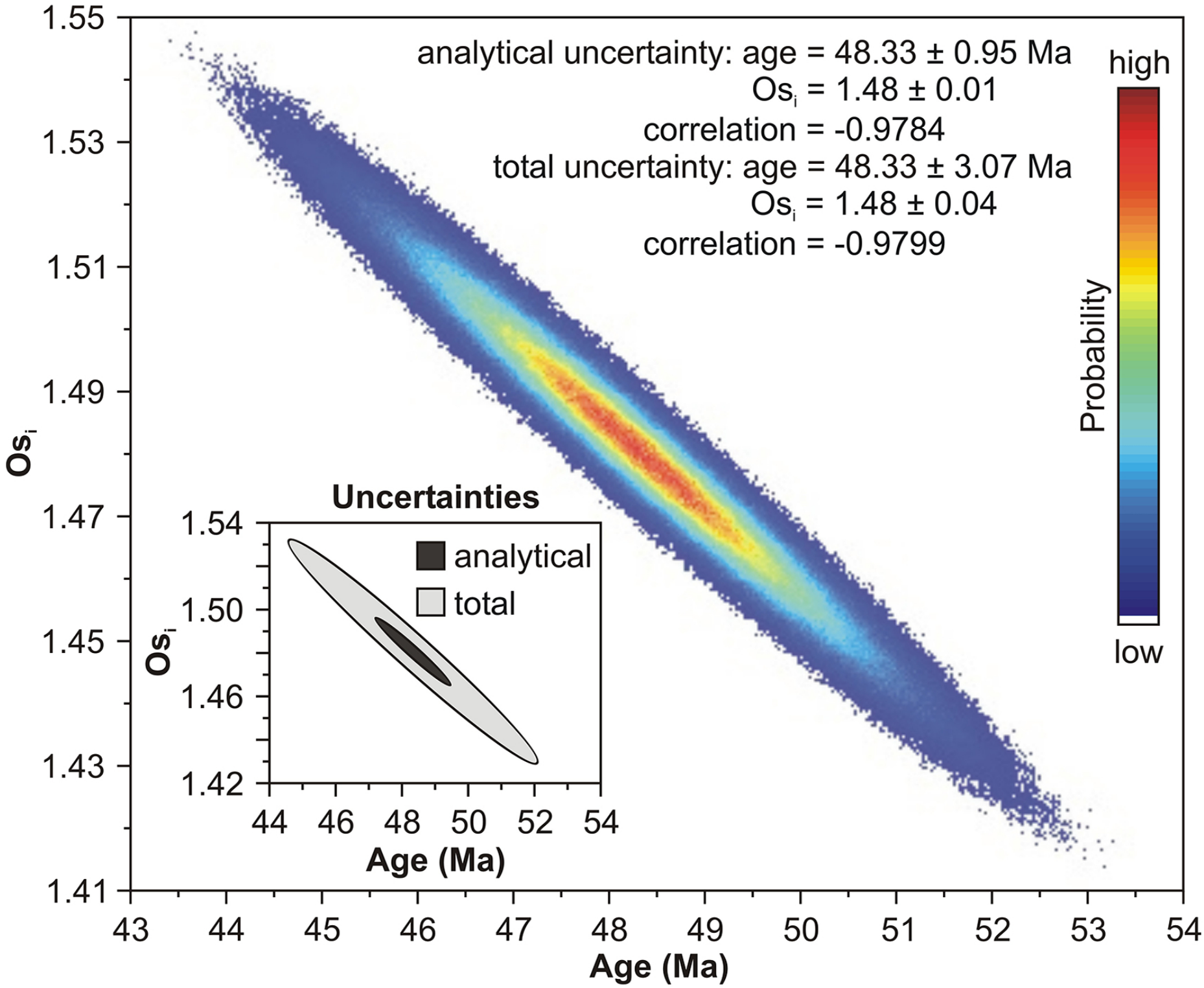
analytical uncertainty: age = 48.33 ± 0.95 Ma
Os$_i$ = 1.48 ± 0.01
correlation = -0.9784
total uncertainty: age = 48.33 ± 3.07 Ma
Os$_i$ = 1.48 ± 0.04
correlation = -0.9799
high
Probability
low
Os$_i$
Age (Ma)
Uncertainties
analytical
total
Os$_i$
Age (Ma)

Figure 6

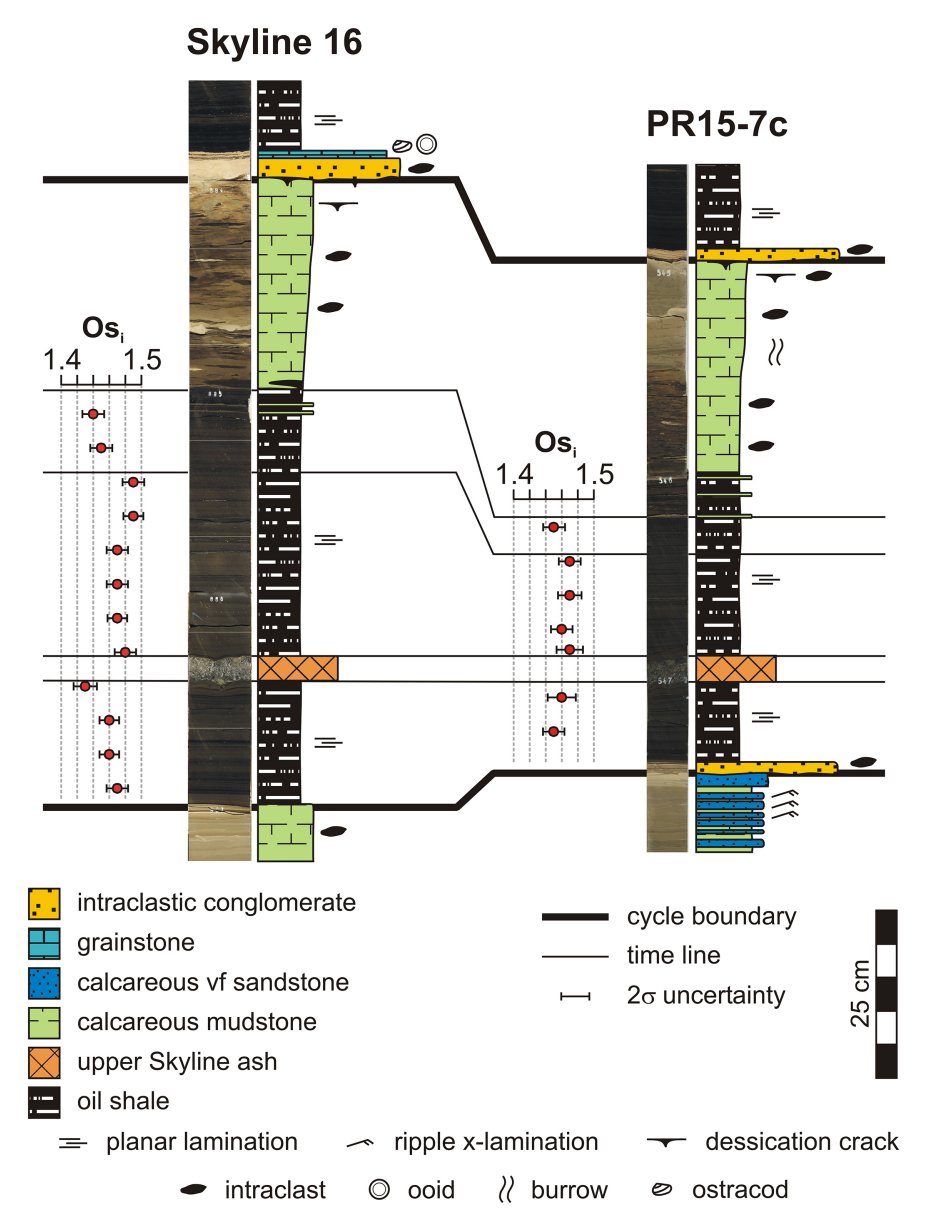
Skyline 16
PR15-7c
Os$_i$
1.4 1.5
Os$_i$
1.4 1.5
intraclastic conglomerate
grainstone
calcareous vf sandstone
calcareous mudstone
upper Skyline ash
oil shale
cycle boundary
time line
2σ uncertainty
25 cm
planar lamination
ripple x-lamination
dessication crack
intraclast
ooid
burrow
ostracod

Figure 7

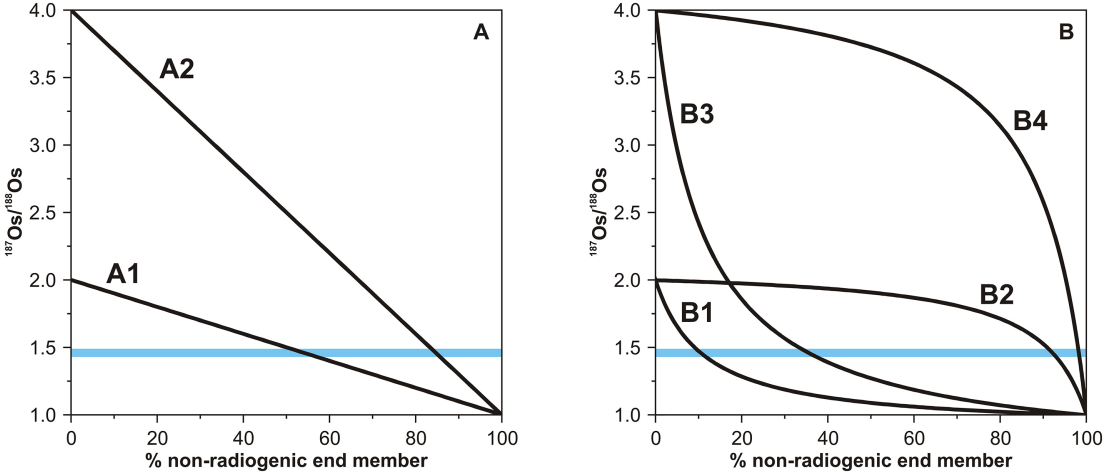
A
A2
A1
4.0
3.5
3.0
2.5
2.0
1.5
1.0
$^{187}Os/^{188}Os$
0
20
40
60
80
100
% non-radiogenic end member
B
B3
B4
B2
B1
4.0
3.5
3.0
2.5
2.0
1.5
1.0
$^{187}Os/^{188}Os$
0
20
40
60
80
100
% non-radiogenic end member

Figure 8